



# Phase Transformations in $\gamma$ -Aluminide, Ti–46.5Al– $x$ Nb– $y$ Cr– $z$ Mo–0.3B ( $x = 3.5, 5; y, z = 0, 1, 2; y + z = 2$ ) Alloys

Naga Sruthi Neelam<sup>1,2</sup> · S. Banumathy<sup>1</sup> · G. V. S. Nageswara Rao<sup>2</sup> · A. K. Singh<sup>1</sup> · A. Bhattacharjee<sup>1</sup>

Received: 21 January 2020 / Revised: 18 April 2020 / Accepted: 11 May 2020 / Published online: 27 May 2020  
© ASM International 2020

## Abstract

The response of as-cast microstructure of six  $\gamma$  TiAl alloys with 46.5 at.% Al and varying Nb, Cr and Mo additions in the temperature range of 1150–1400 °C in water quenched and furnace cooled condition has been studied. The microstructural constituents, their morphologies and phase fractions along with their hardness were determined. The microstructural features at various temperatures were correlated with the transformation temperatures obtained through DSC. The alloy system investigated lies in a two phase  $\alpha + \beta$  field from about 1430 °C down to about 1288–1272 °C. A three phase region below the two phase field exists, with the eutectoid temperature lying in the range of 1155–1076 °C. The volume fraction of  $\beta$ /B2 phase in water quenched condition is generally higher than in furnace cooled condition as sufficient time is allowed for its decomposition in later condition and reaches its equilibrium which in turn decreases the hardness of alloys in furnace cooled condition.

**Keywords** Intermetallics · Phase transformation · Heat treatment · Aero-engine components

## Introduction

$\gamma$ -TiAl alloys being complex multi-phase materials with good high temperature properties are of great interest for specific high temperature applications such as components of aero-engines and parts of high performance cars [1, 2]. It is well known that the mechanical properties of these alloys such as wear resistance, fatigue and creep resistance are highly sensitive to microstructure [1–3]. These alloys primarily contain three intermetallic phases,  $\gamma$ -TiAl,  $\alpha_2$ -Ti<sub>3</sub>Al and  $\beta$ /B2, where  $\gamma$  phase has an ordered L1<sub>0</sub> type face centered tetragonal (fct) crystal structure while  $\alpha_2$  has a DO<sub>19</sub> hexagonal close packed structure and  $\beta$ /B2, a bcc structure. These phases may be ordered at ambient temperatures [4] and have fairly complex phase diagrams. To establish a correlation between microstructure and mechanical properties, it is essential to understand the occurrence of these constituent phases ( $\gamma$ ,  $\alpha_2$  and  $\beta$ ) as a function of temperature and their transformation kinetics. Quite a lot of research has

been carried out to understand the phase transformations in binary Ti–Al alloys for more than a decade [5–7]. However, more systematic research is required for better understanding of phase transformations and heat treatment parameters which in turn helps in the determination of microstructure and mechanical property relationships in ternary and quaternary alloys as alloying additions also influence the amount of phases and their thermal stability [1, 8].

A study has therefore been planned to understand the effect of composition variation of  $\gamma$  alloys containing 46.5 at.% Al. As these alloys are deformable at higher temperatures, it is pertinent to investigate the effect of alloying additions on microstructures in both the as-cast, as well as in heat treated conditions and to evaluate its effect on mechanical properties in a standard heat treatment condition. Part of the work, describing the solidification behavior of these alloys in as-cast condition has been reported elsewhere [9]. The present work investigates the effect of alloying additions (Nb, Cr and Mo) on the phase transformation behavior of Ti–46.5Al– $x$ Nb– $y$ Cr– $z$ Mo–0.3B alloys, where ( $x = 3.5, 5$ ; and  $y, z = 0, 1, 2$  and  $y + z = 2$ ). The alloys with a systematic variation of constituent elements have been imparted heat treatments at various temperatures of interest and have been cooled at two different rates. The microstructures thus obtained after various heat treatments have been discussed

✉ Naga Sruthi Neelam  
neelamnagasruthi16@gmail.com

<sup>1</sup> Defence Metallurgical Research Laboratory,  
Kanchanbagh, Hyderabad 500 058, India

<sup>2</sup> Department of Metallurgical and Materials Engineering, NIT  
Warangal, Warangal 506 004, India

and utilized to understand the phase equilibria in different temperature regimes.

## Experimental Procedures

Phase transformations in Ti–46.5Al– $x$ Nb– $y$ Cr– $z$ Mo–0.3B (all at.%) alloys have been investigated in the present study with a systematic variation of Nb, Cr and Mo. The alloys containing ( $x=3.5, 5$ ) Nb; ( $y=0, 1$  and  $2$ ) Cr and ( $z=0, 1$  and  $2$ ) Mo and  $y+z=2$  were melted in Vacuum arc melting furnace (make: Vacuum Techniques, Bangalore, India) in the form of pancakes. High purity Ti sponge, Al, Cr, Nb–Al master alloy, Mo–Al master alloy and Boron powder were used for melting. The nominal and analyzed chemical compositions of all the alloys (in at.%) along with interstitial contents are given in Table 1. The chemical compositions have been determined by Inductively Coupled Plasma-Optical Emission Spectroscopy (ICP-OES) of Jobin–Yvon Make, France and the gaseous elements have been analyzed in Leco<sup>®</sup> analyser.

Samples were cut from the as-cast pancakes of 3 mm length and 2 mm × 2 mm in cross section and were placed in an alumina crucible and heated up to 1450 °C at a rate of 20 °C per minute in argon atmosphere in Netzsch GmbH make STA 449 Jupiter, differential calorimeter. After attaining the temperature, it was cooled at the same rate and the exothermic and endothermic reactions were recorded and thereby the phase transformations temperatures of the alloys were determined.

The samples machined from the pancakes of all the alloys were imparted systematic heat treatments at different temperatures. They were held for 4 h (hrs) and cooled at two different rates from the heat treatment temperatures to determine the phase constituents of the alloys at different temperatures after cooling to room temperature (Table 2). The heat treatments were carried out in a Bysakh<sup>®</sup> make muffle furnace in air. The temperature was controlled within the range of ± 5 °C in the heat treatment furnace. The temperatures of the samples during heat treatment were monitored by a (R type: Platinum-13% Rhodium) job thermo-couple.

The samples were coated with Deltaglaz FB 412<sup>®</sup> colloidal glass solution of Henkel make to minimize the oxidized layer during heat treatment. Moreover, the surface of the specimens was ground off before examining their microstructure. The microstructural examination of all the samples were carried out in a scanning electron microscope (SEM) in BSE mode (FEI make Quanta 400) and the phase identification were carried out by X-ray diffraction (XRD) in a Philips make, PW3020 model equipment. The fractions of different microstructural constituents present at different heat treatment temperatures were determined using ImageJ<sup>®</sup> analysis software and also verified manually using point count method [10].

## Results

The experimental alloys in the present investigation for discussion have been divided into two categories: (a) 3.5 at.% Nb and (b) 5 at.% Nb containing alloys. Figures 1 and 2 show the microstructures of the alloys Ti–46.5Al–3.5Nb–2Cr–0.3B (A1), Ti–46.5Al–3.5Nb–1Cr–1Mo–0.3B (A2) and Ti–46.5Al–3.5Nb–2Mo–0.3B (A3), whereas Figs. 3 and 4 of alloys Ti–46.5Al–5Nb–2Cr–0.3B (A4), Ti–46.5Al–5Nb–1Cr–1Mo–0.3B (A5) and Ti–46.5Al–5Nb–2Mo–0.3B (A6) after heat treatment at various temperatures and then cooled to room temperature

**Table 2** Different heat treatment cycles that were imparted to the  $\gamma$ -TiAl alloys

S. no.	Temperature, °C	Soaking time, h	Cooling condition
1	1150	4	Water quenching (WQ) and furnace cooling (FC)
2	1200	4	WQ and FC
3	1250	4	WQ and FC
4	1300	4	WQ and FC
5	1350	4	WQ and FC
6	1400	4	WQ and FC

**Table 1** Composition of the  $\gamma$ -TiAl alloys in at.%

Alloy	Elements, at.%							Interstitials, at.%		
	Ti	Al	Nb	Cr	Mo	B	C	O	N	
A1	47.7 (50.23)	46.5 (43.29)	3.5 (3.68)	2 (2.03)	– (0.028)	0.3 (0.21)	0.21	0.3	0.008	
A2	47.7 (49.88)	46.5 (44.37)	3.5 (3.45)	1 (1.06)	1 (0.81)	0.3 (0.32)	0.08	0.13	0.005	
A3	47.7 (51.12)	46.5 (42.60)	3.5 (3.38)	– (0.08)	2 (2.02)	0.3 (0.33)	0.20	0.2	0.005	
A4	46.2 (47.25)	46.5 (42.87)	5 (4.62)	2 (1.99)	– (0.037)	0.3 (0.29)	0.10	0.18	0.005	
A5	46.2 (49.05)	46.5 (43.72)	5 (4.61)	1 (1.04)	1 (1.10)	0.3 (0.25)	0.10	0.23	0.005	
A6	46.2 (48.42)	46.5 (44.11)	5 (4.64)	– (0.04)	2 (2.04)	0.3 (0.39)	0.11	0.19	0.002	

Chemical composition of alloys analyzed using ICP-OES technique are given in parenthesis

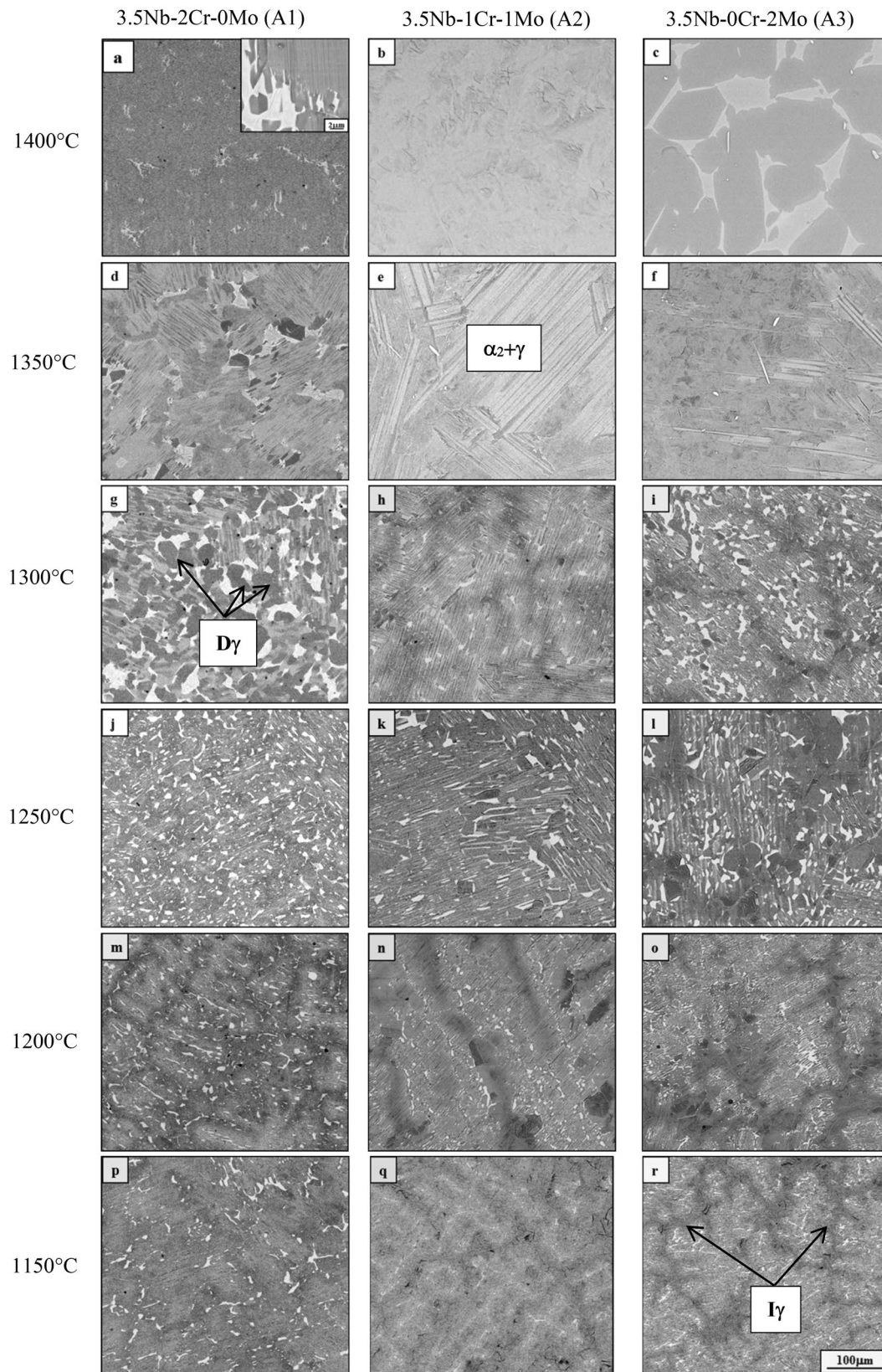


**Fig. 1** The SEM micrographs of alloys A1, A2 and A3 as a function of temperature followed by WQ

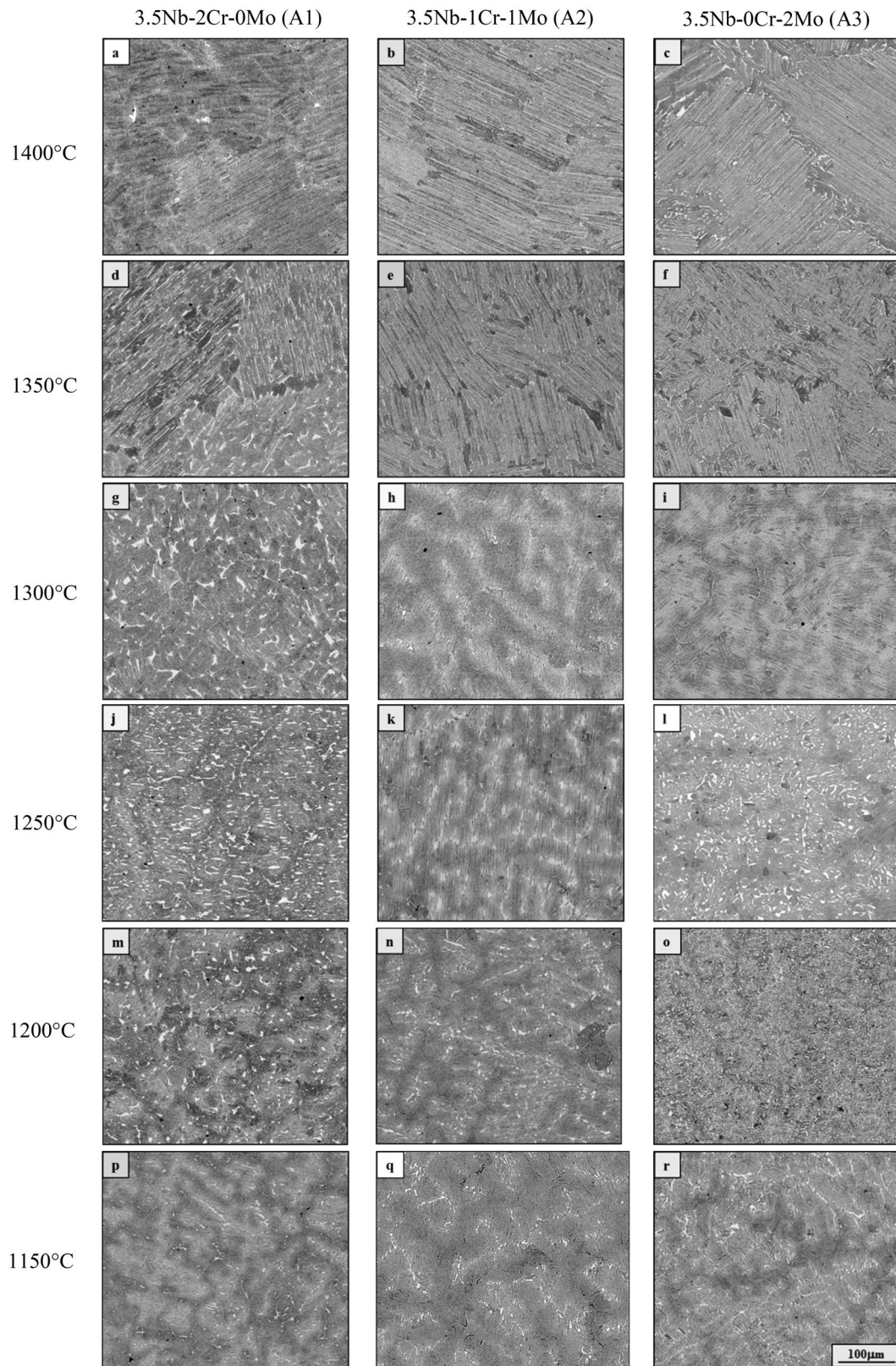


**Fig. 2** The SEM micrographs of alloys A1, A2 and A3 as a function of temperature followed by FC

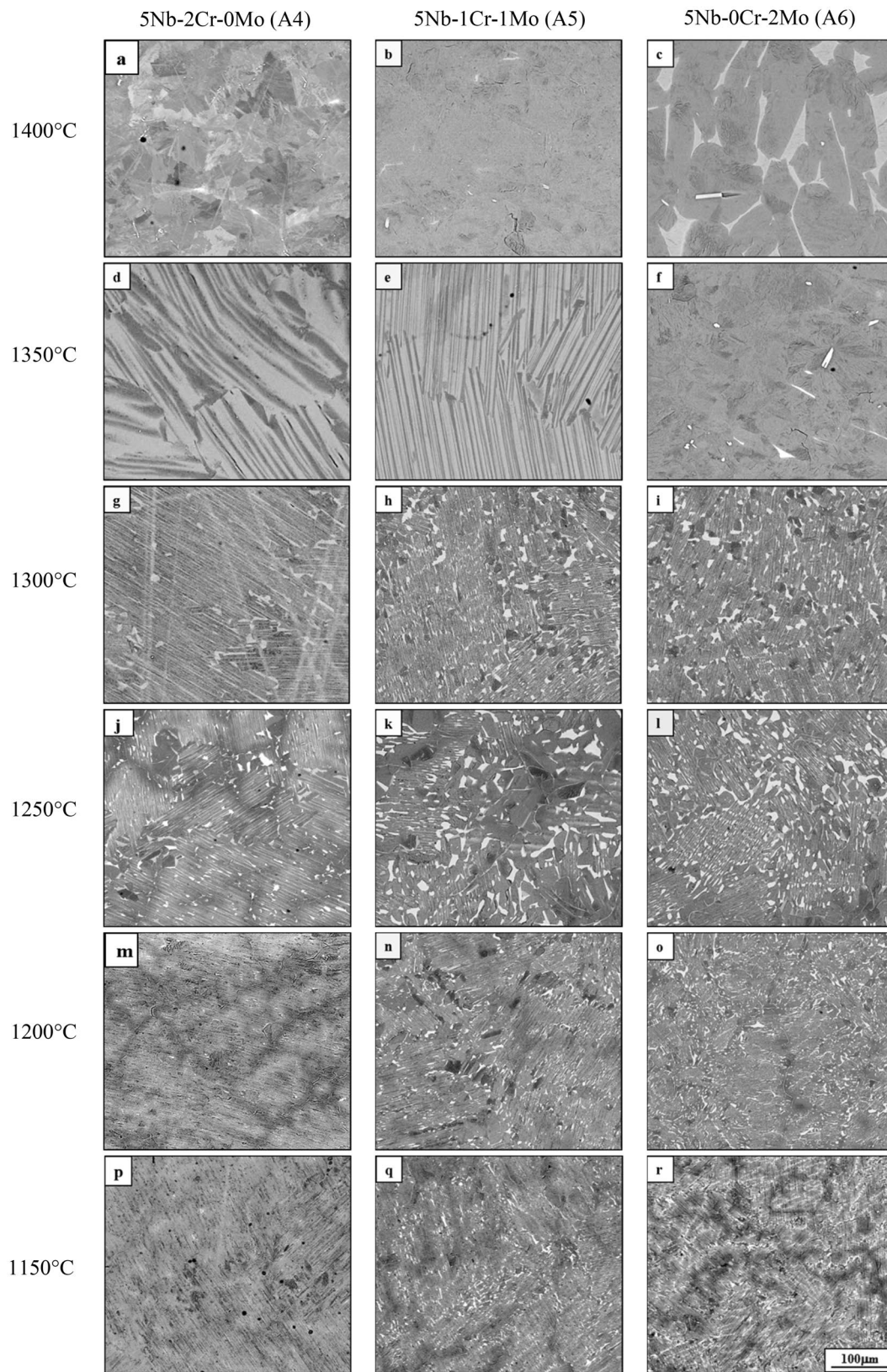


**Fig. 3** The SEM micrographs of alloys A4, A5 and A6 as a function of temperature followed by WQ

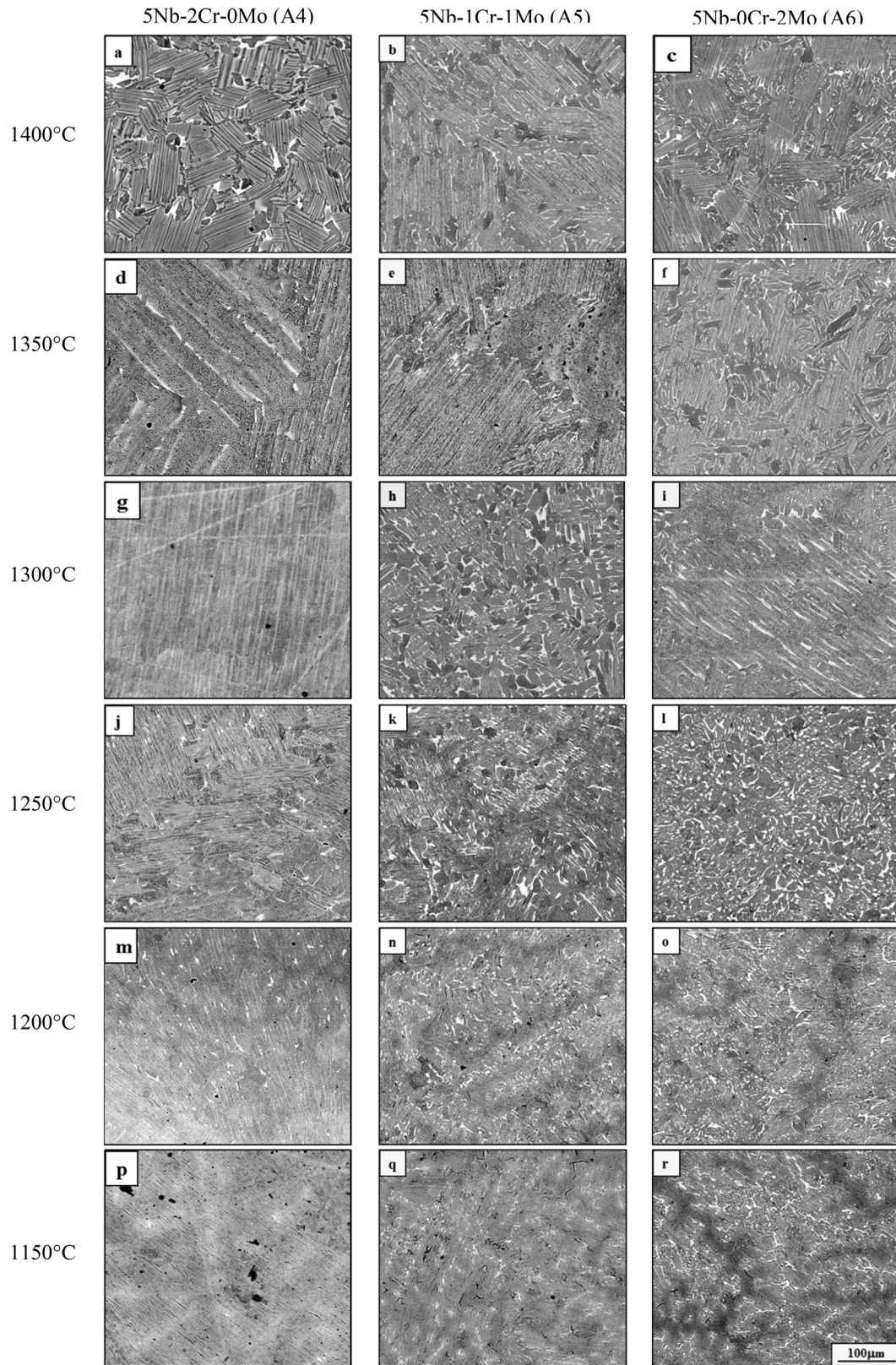


**Fig. 4** The SEM micrographs of alloys A4, A5 and A6 as a function of temperature followed by FC

by water quenching (WQ) and furnace cooling (FC), respectively. The dendritic structure observed in the as-cast condition is also observed during heat treatment for all the alloys [9].

**Alloys Containing 3.5 at.% Nb After Heat Treatment at Various Heat Treatment Temperatures**

**Water Quenched Condition (Fig. 1)**

The BSE SEM microstructure of alloy A1 exhibits a two phase contrast of bright and gray after heat treatment at

1400 °C for 4 h followed by WQ (Fig. 1a). The bright phase is identified as  $\beta$  and gray as  $\alpha/\alpha_2$  from previous studies [8, 9, 11]. After treatment at 1350 °C,  $\alpha_2 + \gamma$  lamellar colonies with equiaxed  $\alpha_2$  and  $\gamma$  grains along the colony boundaries are observed (Fig. 1d). Bright  $\beta$  phase is also seen along the colony boundaries (Fig. 1d). With the decrease in heat treatment temperature to 1300 °C, the lamellar colony size seem to have decreased significantly and equiaxed  $\gamma$  phase is observed and  $\beta$  phase is seen around the grain boundaries as shown in Fig. 1g. The  $\beta$  and  $\gamma$  phase fraction has also increased (Table 3). At 1250 °C, though a three phase  $\beta$ ,  $\gamma$  and  $\alpha_2$  structure is observed, their morphology is quite

**Table 3** The quantitative analysis of volume fractions of  $\beta$ ,  $\alpha_2$  and  $\gamma$  phases at various heat treatments and cooling rates

Alloy	Temperature, °C	$\beta/B2$ , %		$\alpha_2$ , %		$\gamma$ , %	
		WQ	FC	WQ	FC	WQ	FC
A1	1150	7.72	4.00	45.97	42.26	51.09	53.06
	1200	6.71	3.11	43.09	43.34	52.17	53.76
	1250	6.35	4.69	43.78	45.97	49.98	49.67
	1300	12.40	5.22	35.36	44.23	53.31	52.64
	1350	7.85	3.52	45.34	39.06	47.77	57.28
	1400	7.72	2.13	54.41	51.28	37.87	47.69
A2	1150	7.11	5.96	45.98	46.8	48.02	48.91
	1200	4.89	3.70	49.14	46.87	46.58	50.94
	1250	7.46	4.06	42.63	44.38	50.72	51.58
	1300	2.86	1.47	47.68	40.03	50.53	49.71
	1350	1.02	2.94	41.27	42.28	58.19	53.51
	1400	0	2.0	79.5	46.13	20.5	48.65
A3	1150	8.05	6.52	42.16	44.83	49.07	48.27
	1200	7.08	6.74	41.16	43.03	51.63	52.32
	1250	8.35	7.61	42.15	42.51	50.91	50.47
	1300	12.30	1.11	40.36	46.04	48.85	52.58
	1350	1.11	6.26	33.93	42.97	66.98	50.82
	1400	11.79	5.70	88.21	44.34	0	49.87
A4	1150	5.37	2.33	48.80	47.54	46.47	50.13
	1200	3.46	1.08	46.25	46.06	50.36	51.76
	1250	4.06	1.79	44.65	46.38	51.29	51.83
	1300	0.30	1.25	50.76	48.50	48.94	50.25
	1350	0.35	1.23	45.78	46.98	54.22	51.79
	1400	0.37	4.07	43.73	42.38	55.78	53.55
A5	1150	7.18	2.47	42.27	48.16	51.72	50.03
	1200	7.45	3.30	44.44	47.81	49.60	48.89
	1250	8.59	3.87	42.02	48.07	49.78	49.28
	1300	7.09	6.90	43.02	45.06	49.73	48.01
	1350	1.29	3.28	49.90	47.54	50.01	48.69
	1400	0.27	3.65	49.08	47.26	49.71	48.35
A6	1150	8.90	4.01	42.69	46.86	49.73	49.36
	1200	8.15	12.53	41.18	40.28	51.96	47.33
	1250	7.05	8.39	44.33	41.46	49.50	48.94
	1300	5.01	2.88	44.13	48.91	50.78	49.55
	1350	2.88	7.87	48.91	44.28	49.55	48.17
	1400	4.36	6.36	49.38	42.38	57.11	51.26

different from that observed at 1300 °C. Fine lamellar structure of  $\alpha_2 + \gamma$  with  $\beta$  phase at the colony boundaries and within the lamellar structure is observed as shown in Fig. 1j. With the decrease in temperature from 1300 to 1250 °C, the equiaxed  $\gamma$  and  $\alpha_2$  appear to have disappeared, and most of the  $\beta$  phase appears as fine and elongated as compared to blocky/equiaxed at the boundaries (Fig. 1j). The alloy has similar microstructures at 1200 and 1150 °C, as shown in Fig. 1m and p, except for the decrease in  $\beta$  phase fraction (Table 3). It may be observed that dendritic  $\beta$  and inter-dendritic  $\gamma$  ( $I\gamma$ ) structure from as-cast condition is retained even after heat treatment [8]. The presence of  $\beta$  along the boundaries of inter-dendritic  $\gamma$  is observed (Fig. 1p).

At 1400 °C, alloy A2 exhibits a two phase, dark  $\gamma$  and gray  $\alpha_2$  contrast (Fig. 1b). After heat treatment at 1350 °C, a coarse  $\alpha_2 + \gamma$  lamellar structure is observed (Fig. 1e) whereas at 1300 °C, a fine lamellar structure along with  $\beta$  phase at colony boundaries is clearly seen (Fig. 1h). With the decrease in temperature to 1250 °C, again a lamellar structure is seen (Fig. 1k) and an increase in  $\beta$  phase fraction (Table 3) is observed which occur at colony as well as at lamellae boundaries. At 1200 °C, alloy exhibits dendritic  $\beta$  and inter-dendritic  $\gamma$ , along with fine lamellar structure (Fig. 1n). The presence of  $\beta$  phase along the inter-dendritic  $\gamma$  phase and within the lamellae is also seen. A similar fine structure is observed at 1150 °C as shown in Fig. 1q.

Alloy A3 exhibits a two phase structure of  $\beta$  around the boundaries of  $\alpha$  grains at 1400 °C which is clearly evident in Fig. 1c. At 1350 °C, along with lamellar structure, a few fine equiaxed  $\gamma$  can also be observed (Fig. 1f). With the decrease in temperature to 1300 °C, a fine lamellar  $\alpha_2 + \gamma$  structure along with equiaxed  $\beta$  and  $\gamma$  grains are evident in Fig. 1i. A similar coarsened structure is seen after a heat treatment at 1250 °C (Fig. 1l). At 1200 and 1150 °C, the structure is similar to that of the alloy A2, except for the increase in  $\beta$  phase fraction (Table 3).

The phases formed at each temperature and retained at room temperature after cooling at two different rates have been identified through XRD studies. A typical XRD pattern, showing  $\beta/B2$ ,  $\gamma$  and  $\alpha/\alpha_2$  at 1150 °C in WQ and FC conditions are shown in Fig. 5 and the volume fraction of different phases present at different temperatures have been determined from the micrographs and are given in Table 3.

**Table 4** The chemical composition of phases in alloy A6 at 1400 °C/FC by EPMA

Phases	Elements			
	Ti	Al	Nb	Mo
$\beta$	46.84	43.90	5.76	3.52
$\alpha$	64.35	33.80	1.54	0.31
$\gamma$	45.25	47.61	5.26	1.80

## Furnace Cooled Condition (Fig. 2)

Alloy A1 exhibits a fine lamellar structure after furnace cooling from 1400 °C (Fig. 2a) with negligible amount of  $\beta$  phase, whereas at 1350 °C, a similar microstructure with  $\beta$  phase along the colony boundaries and within the lamellae was noticed (Fig. 2d). The increase in  $\beta$  phase fraction is clearly seen and can also be inferred from Table 3. As the temperature decreases to 1300 °C, further increase in  $\beta$  phase was observed accompanied by the refinement of lamellar structure (Fig. 2g), unlike the equiaxed structure in water quenched condition (Fig. 1g). At temperatures 1250, 1200, and 1150 °C (Fig. 2j, m, and p), the structure was similar to that of the WQ condition (Fig. 1j, m, and p), except for lower  $\beta$  phase fraction (Table 3).

The microstructure of alloy A2 after heat treating at 1400 °C was similar to that of the alloy A1, with fine  $\alpha_2 + \gamma$  lamellae with very low fraction of fine  $\beta$  at the colony boundaries (Fig. 2b and Table 3). At 1350 °C, the presence of  $\beta$  at the colony boundaries was more prominent. The lamellae were coarser in comparison to those at 1400 °C and a few elongated  $\gamma$  grains along the colony boundaries were observed (Fig. 2e). The response of alloy A2 to heat treatments at 1300 and 1250 °C was almost similar (Fig. 2h, k) and it resulted in a fine lamellar structure. Dendritic  $\beta$  and inter-dendritic  $\gamma$  (Fig. 2h and k) and the increase in  $\beta$  phase with decrease in temperature were clearly observed (Table 3). Apart from the increase in  $\beta$  phase fraction (Table 3), the microstructures of the alloy A2 at 1200 and 1250 °C (Fig. 2n and q) were identical to that of the alloy A1 (Fig. 2m and p). At 1400 and 1350 °C, alloy A3 exhibited a similar microstructure (Fig. 2c and f) as that of alloy A2 (Fig. 2b and e) with an increase in  $\beta$  phase fraction (Table 3). Alloy A3 has a lamellar  $\alpha_2 + \gamma$  microstructure of

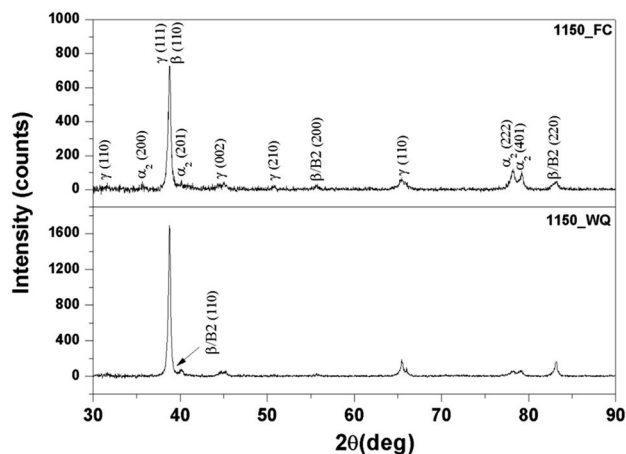


**Fig. 5** The typical XRD plot showing the presence of  $\beta/B2$ ,  $\alpha/\alpha_2$  and  $\gamma$  phases in alloy A1 after heat treatment at 1150 °C and cooling at two different rates



after treatment at 1300 °C, whereas at 1250 °C, a fine lamellar structure with equiaxed  $\gamma$  and  $\beta$  grains was seen in Fig. 2i, and an increase in  $\beta$  phase fraction (Table 3). At 1200 °C, refinement of the microstructure was clearly evident (Fig. 2l) and at 1150 °C (Fig. 2r), a dendritic structure similar to that of the alloys A1 and A2 was observed.

## Alloys with 5 at.% Nb at Various Heat Treatment Temperatures

### Water Quenched Condition (Fig. 3)

After heat treatment at 1400 °C followed by WQ, alloy A4 exhibited a three phase contrast (Fig. 3a). The presence of  $\beta$  along the grain boundaries of  $\gamma/\alpha_2$  was clearly seen along with some inside the grains, whereas at 1350 °C, a coarser lamellar structure of  $\alpha_2 + \gamma$  was observed (Fig. 3d). A finer lamellar microstructure after heat treatment at 1350 and 1300 °C was observed along with the presence of  $\beta$  phase at the colony boundaries (Fig. 3g). After 1250 °C treatment, the presence of elongated  $\beta$  and  $\gamma$  was evident along with fine lamellar structure (Fig. 3j). With the decrease in heat treatment temperature from 1250 to 1200 °C, slightly coarser lamellar structure with elongated  $\gamma$  and  $\beta$  grains at the colony boundaries and triple points was observed (Fig. 3m). At 1150 °C, a dendritic  $\beta$  and inter-dendritic  $\gamma$  and  $\alpha_2 + \gamma$  lamellar structure was clearly noticed (Fig. 3p) and the presence of these phases has been identified by XRD and their phase fractions are given in Table 3.

Figure 3b, e, h, k, n, and p shows the microstructural evolution of alloy A5 after heat treatment at 1400 to 1150 °C followed by WQ. The alloy exhibited almost a two phase microstructure of  $\alpha/\alpha_2$  and  $\gamma$  with negligible amount of  $\beta$  (Fig. 3b) after treatment at 1400 °C. At 1350 °C, fine lamellar structure with large colonies (Fig. 3e) was observed similar to that of alloy A1 (Fig. 3d), whereas after treatment at 1300 °C, a finer colony consisting of  $\alpha_2 + \gamma$  lamellae were seen (Fig. 3h). Both elongated and equiaxed grains of  $\beta$  and  $\gamma$  were observed at the colony boundaries and elongated  $\beta$  were seen within the lamellae also. A similar structure was observed at 1250 °C, except for the coarsening of lamellae and  $\beta$  phase (Fig. 3k). After treatment at 1200 and 1150 °C, apart from the refinement of the lamellar colony size, the microstructures were identical (Fig. 3n and p). Alloy A6 exhibited a three phase contrast of  $\beta$ ,  $\alpha_2$  and  $\gamma$ , with  $\beta$  phase being present at grain boundaries at 1400 °C (Fig. 3c). At 1350 °C, unlike alloys A4 and A5 which exhibited a lamellar structure, a two phase  $\gamma$  and  $\alpha_2$  structure with negligible amounts of  $\beta$  was observed (Fig. 3f). After heat treatment at temperatures, 1300 to 1150 °C, alloy A6 reflects a microstructure similar to that of the alloy A5 except a slightly higher  $\beta$  volume fraction at corresponding heat treatment temperatures (Fig. 3i, l, o, and r) and Table 3).

### Furnace Cooled Condition (Fig. 4)

Alloy A4 exhibited a  $\alpha_2 + \gamma$  lamellar microstructure for all the heat treatment temperatures, i.e., from 1400 to 1150 °C, followed by FC (Fig. 4a, d, g, j, m, and p) with negligible amount of  $\beta$  phase. After heat treatment at 1400 °C and FC, along with lamellar structure, equiaxed  $\gamma$  at the colony boundaries and slight amount of elongated  $\beta$  at the lamellar boundaries were seen (Fig. 4a). It was observed that with the decrease in heat treatment temperature from 1400 to 1150 °C, refinement of lamellar structure takes place (Fig. 4a, d, g, j, m, and p). The alloy A5 on treatment at 1400 °C, results in  $\alpha_2 + \gamma$  lamellar structure with  $\beta$  phase along the colony boundaries and within the lamellae and there was also presence of some elongated/equiaxed  $\gamma$  grains (Fig. 4b). Along with  $\alpha_2 + \gamma$  lamellar structure and  $\beta$  phase, a massive structure was also observed at 1350 °C in alloy A5 (Fig. 4e). Except for the decrease in  $\beta$  phase fraction (Table 3), the response of the alloy to heat treatments at 1300, 1250, 1200, and 1150 °C followed by FC (Fig. 4h, k, n, and p) was similar to that in WQ condition (Fig. 3h, k, n, and p).

Microstructure of the alloy A6 showed the presence of  $\alpha/\alpha_2$  and  $\gamma$  grains in  $\beta$  matrix after heat treatment at 1400 °C (Fig. 4c). After heat treatment at 1350 °C, a coarser lamellar structure with few equiaxed  $\alpha_2$  and  $\gamma$  grains were observed (Fig. 4o). These equiaxed grains were surrounded by the  $\beta$  phase (Fig. 4f). The equiaxed structure disappeared and formed a fine lamellar structure as the temperature of heat treatment decreased from 1350 to 1300 °C (Fig. 4i). The microstructure at 1250, 1200, and 1150 °C after FC was comparable to that in WQ condition as shown in Fig. 4l, o, and r) and Fig. 3l, o, and r). The only difference was the decrease in  $\beta$  phase fraction on FC as compared to that in WQ condition (Table 3). The quantitative microanalysis of the phases present in alloy A6 at 1400 °C is given in Table 4. Though the microstructural constituents were same in WQ and FC conditions for all the alloys, there exists a significant variation in the volume fractions of the phases which is given in Table 3.

## Discussion

The solidification behavior of all the six alloys in as-cast condition has been studied and reported, elsewhere [9]. All the alloys solidify through  $L + \beta \rightarrow \beta + \alpha$  phase field rather than the  $L + \beta \rightarrow \alpha$ , due to the addition of  $\beta$  stabilizing elements. The first and last solids to form in all the alloys are  $\beta$  and  $\gamma$  phases, respectively. All the alloys pass through a  $\beta + \alpha + \gamma$  phase field. The reactions  $\beta \rightarrow \beta + \gamma$ ,  $\alpha + \beta \rightarrow \gamma$  and  $\alpha \rightarrow \alpha_2 + \gamma$  give rise to precipitation of  $\gamma$  within the  $\beta$  phase,

peritectoid rim of  $\gamma$  around  $\beta$  and lamellar microstructures, respectively, in as-cast condition [9].

The existence of different constituent phases present in the various alloy compositions observed after different heat treatments in the present study will be discussed at the backdrop of different related phase diagrams (Figs. 6 and 7) that have been reported by various authors for  $\gamma$ -TiAl-based alloy systems [12, 13] along with the DSC results obtained in the present study. The different transformation temperatures obtained for the various compositions of the alloys in the present study in the DSC scans are given in Table 5. A typical DSC scan for the alloy A1 is shown in Fig. 8, and a schematic phase diagram for the present alloy system studied is given in Fig. 9.

### Transformations (DSC)

The various transformation temperatures of all the six alloys from DSC analysis are given in Table 5. Alloy A1 (3.5 at.% Nb) enters into  $\alpha + \beta$  region from  $\beta$  region at 1430 °C (Table 5), which is lower than the reported,  $\beta \rightarrow \alpha + \beta$  transformation temperature ( $T_\beta$ ) of ~ 1450 °C for binary alloys [14]. This change in  $T_\beta$  can be attributed to the addition of beta stabilizing elements Nb, Cr and Mo. It has been reported that the  $\beta$  stabilizing elements (Cr, Mo and V) introduces regular shift of phase boundaries. The effect of these elements on the phase boundaries of binary Ti–Al system has been reported and is given in Fig. 7 [14]. These alloying additions lower the  $\beta \rightarrow \alpha$  transformation temperatures. In contrast, higher Al content leads to the

expansion of single phase  $\beta$  and two phase  $\alpha + \beta$  regions. Simultaneously, along with two phase  $\alpha_2 + \beta$  region, a three phase,  $\alpha_2 + \beta + \gamma$  region also appears, and its boundaries shift in the direction of lower Al content [13]. A schematic phase diagram for the alloy system under study was drawn and is shown in Fig. 9. For the alloy A1, the  $\beta \rightarrow \alpha + \beta$  transformation occurs at 1430 °C and there is hardly any variation in temperature across the different alloy compositions (A1 to A3) (Table 5). At 1272 °C, the alloy A1 enters a three-phase region ( $\alpha + \beta \rightarrow \alpha + \beta + \gamma$ ) and at around 1235 °C, the  $\beta \rightarrow B2$  ordering reaction occurs in the three phase region; then the eutectoid reaction take place for the alloy A1 at 1155 °C, followed by ordering of the  $\alpha$  phase. Therefore, the alloy A1 enters a three phase regime from 1272 °C onwards and continues down to room temperature. Similar phase transformations are observed in case of alloys A2 and A3. It may be concluded from Table 6 that the alloy A1 (containing 2% Cr) has the highest eutectoid temperature of 1155 °C, followed by 1090 °C for A2 (containing 1% each of Cr and Mo), followed by 1076 °C for A3 (containing 2% Mo).  $T_\beta$  of the alloys A2 and A3 are same as that of alloy A1. Similarly,  $\beta \rightarrow B2$  and  $\alpha \rightarrow \alpha + \gamma$  transformation temperatures lie close for the alloys A1, A2 and A3. This indicates that the variation in alloying additions Cr and Mo do not have any significant effect on these transformation temperatures. However, there is a significant and systematic change in the eutectoid transformation temperature ( $T_{eu}$ ) of the alloys. This change can be ascribed to the gradual decrease in Cr content and increase in Mo with Nb and Al

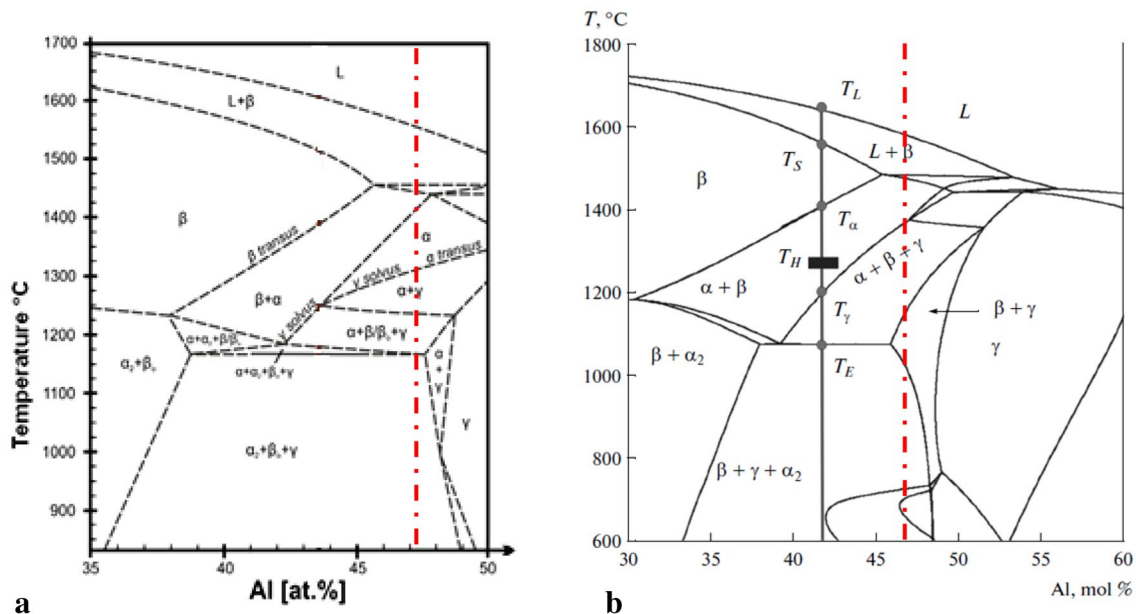


**Fig. 6** Phase diagram: (a) Ti–43.5Al–4Nb–1Mo–0.3B [12] and (b) Ti–Al–Nb–Mo with 4.4 mol.% Nb and 1.1 mol.% Mo [13]. (red dotted line indicates the Al content in the present study) (Color figure online)

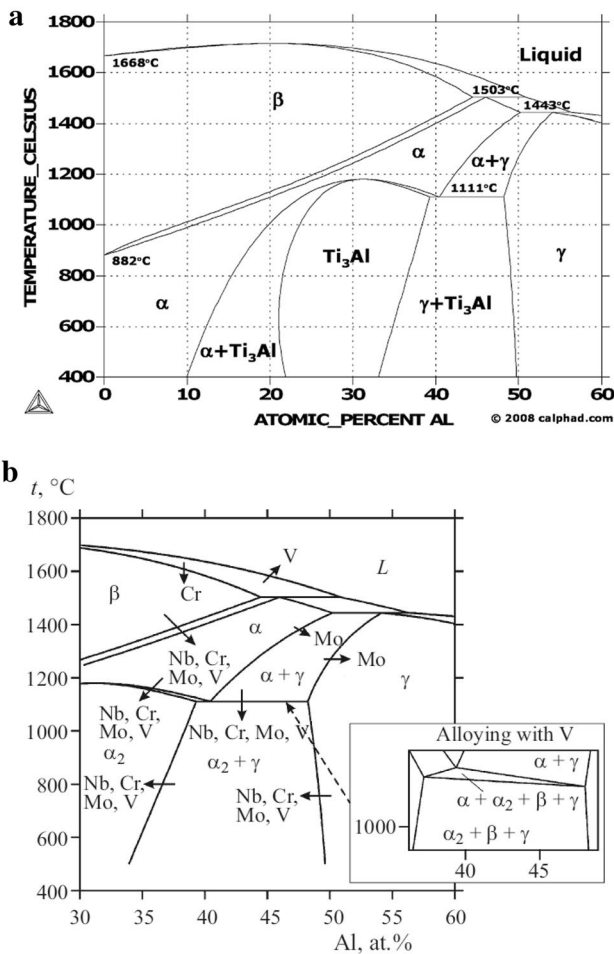


**Fig. 7** (a) Binary phase diagram of Ti–Al system, (b) central part of Ti–Al binary diagram. Arrows indicate the direction of action of alloying elements on phase boundaries. Eutectoid horizontal separation on vanadium addition is shown separately [14]

**Table 5** The transformation temperatures of various alloys by DSC analysis

Alloy	$T_{\beta}$ ( $\beta \rightarrow \alpha + \beta$ )	$T_{\gamma}$ ( $\alpha \rightarrow \alpha + \gamma$ )	$T$ ( $\beta \rightarrow \beta 2$ )	$(T_{eu})$ ( $\alpha \rightarrow \alpha_2 + \beta + \beta 2$ )
A1	1430	1272	1235	1155
A2	1431	1288	1239	1090
A3	1431	1270	1232	1076
A4	1430	1277	1235	1119
A5	1431	1283	1238	1085
A6	1430	1275	1239	1079

remaining constant from A1 to A3. It has been reported that a significant reduction in  $T_{eu}$  occurs with the addition of  $\beta$  stabilizing elements and particularly Mo has a strong effect as a  $\beta$  stabilizer [13] and the present results also support the observation.

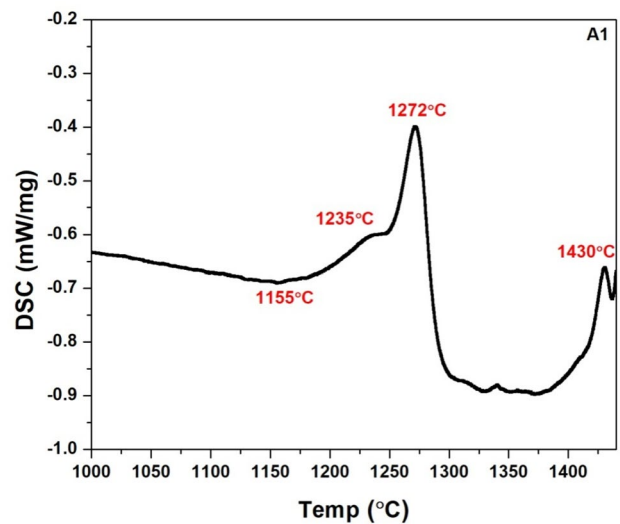


**Fig. 8** A typical differential scanning calorimetry (DSC) plots of the alloy A1

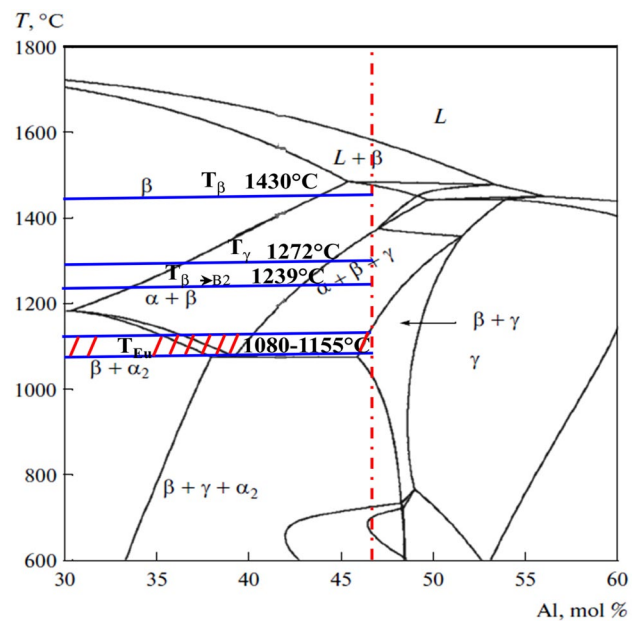


**Fig. 9** A schematic phase diagram of the alloy system under study depicting the various transformation temperatures shown on a Ti–Al–Nb–Mo phase diagram [13]

The alloy A4 with 5 at.% Nb has a  $\beta \rightarrow \alpha + \beta$  transformation temperature of 1430 °C, and A5 and A6 have similar transformation temperatures. The increase in Nb content in A4, A5 and A6 has no significant effect on  $\beta$  phase fraction as it is not a strong beta stabilizer in comparison to Cr and Mo [13]. At 1277 °C, the alloy A4 enters the three phase region and the eutectoid reaction take places at 1119 °C, whereas the alloys A5 and A6 exhibit significant decrease

**Table 6** Hardness values (VHN) of alloys at room temperature after various heat treatments

Alloy	1400 °C		1250 °C		1150 °C	
	WQ	FC	WQ	FC	WQ	FC
A1	383 ± 6.8	288 ± 4.6	318 ± 12.6	267 ± 7.7	290 ± 5.1	260 ± 5.6
A2	350 ± 7.4	254 ± 4.7	276 ± 12.4	273 ± 6.1	314 ± 6.0	295 ± 15.5
A3	381 ± 2.0	273 ± 6.1	297 ± 6.3	287 ± 6.4	338 ± 6.4	310 ± 6.8
A4	407 ± 14.0	289 ± 7.8	291 ± 10.0	241 ± 11.3	324 ± 8.6	266 ± 17.9
A5	346 ± 18.0	246 ± 6.9	276 ± 8.8	257 ± 7.8	321 ± 3.7	295 ± 5.0
A6	326 ± 13.8	291 ± 12.7	291 ± 9.8	265 ± 8.1	336 ± 8.0	329 ± 5.4

in  $T_{eu}$  (Table 5) than that of the alloy A4, similar to the case of 3.5 at.% Nb alloys due to the increase in Mo content [15]. The  $\beta \rightarrow B2$  and  $\alpha \rightarrow \alpha + \gamma$  transformation temperatures are comparable for all the alloys, similar to that of the 3.5 at.% Nb alloy case (Table 5).

As shown in the schematic phase diagram, the various  $\gamma$ -TiAl alloys investigated lie in a two phase  $\alpha + \beta$  field from about 1430 °C down to about 1288–1272 °C (Fig. 9). The  $\beta \rightarrow B2$  transformation temperature of the alloys lies around 1235 °C. The eutectoid transformation temperature appears to decrease quite significantly in the alloys containing both 3.5% Nb and 5% Nb with the increasing addition of Mo.

## Heat Treatments

### 1400 °C

Assuming that the alloy Ti–46.5Al–2Cr–3.5Nb–0.3B (A1) follows the phase diagram shown in Fig. 6, after heat treatment at 1400 °C, a  $\alpha + \beta$  two phase region is expected, whereas the micrographs in WQ condition (Fig. 1a) exhibited a two phase  $\alpha + \beta$  structure with a small region of dark contrast, i.e.,  $\gamma$  phase, and presence of clear  $\gamma$  phase peaks in XRD patterns confirms the presence of three phase structure. The micrographs in FC condition (Fig. 4a) also showed a three phase microstructure supported by the XRD analysis. The presence of a small amount of  $\gamma$  phase after heat treatment at 1400 °C even in WQ condition is the result of decomposition and points to the fact that even a faster cooling rate (WQ) does result in some decomposition. On WQ after holding at 1400 °C, alloy A1 has about 7.6%  $\beta$  phase and rest is  $\alpha$ , but on furnace cooling, the  $\beta$  and  $\alpha$  contents decrease to 2.1 and 51.3%, respectively, and concomitantly the  $\gamma$  content increases. Even though 1400 °C is in two phase,  $\alpha + \beta$  region, presence of all three phases is observed due to the decomposition of  $\alpha + \beta$  to  $\alpha + \beta + \gamma$ . Similar phase transformations are also observed in case of alloys, A2 and A3 (Figs. 1 and 2).

After heat treatment at 1400 °C, the alloy A4 has a significant amount of  $\beta$  phase around the grain boundaries of  $\alpha$  phase and there is also slight amount of  $\gamma$  phase in

the lamellar structure that is a decomposition product both in WQ and FC conditions as observed in the case of alloy, A1. Alloys A5 and A6 also showed similar phase transformations.

### 1350 and 1300 °C

After heat treatment at 1350 °C, the alloy A1 is still in two phase region but due to decomposition,  $\beta$  phase content slightly increases and there is decrease in  $\alpha$  phase and concomitant increase in  $\gamma$ -phase in both WQ and FC conditions and hence the presence of three phases instead of two phase is observed. After heat treatment at 1300 °C (which is in two phase region), the amount of  $\beta$  phase increases in A1 and it forms around the grains and there is decrease and increase in  $\alpha$  and  $\gamma$  phases, respectively.

After heat treatment at 1350 and 1300 °C, the alloy A4 has a  $\alpha + \beta$  lamellar microstructure with slight amount of  $\gamma$  phase which is again a decomposition product in both the WQ and FC conditions. Alloys A5 and A6 having Mo show a higher amount of  $\beta$  at the boundaries at similar heat treatment temperatures and the effect is seen in A5 and A6 from a heat treatment temperature of 1300 °C and below, whereas in A4, it occurs for heat treatment temperature of 1200 °C and below.

### 1250–1150 °C

In the temperature range of 1250–1150 °C, all the alloys exhibit a three phase microstructure as shown in Figs. 1, 2, 3, and 4. For instance, in alloy A1 dendritic structure can be clearly observed from 1150 to 1250 °C (Fig. 1p, m, and j), whereas at high temperatures, i.e., from 1300 to 1400 °C, the dendritic structure is not visible. This is due to the kinetics of  $\beta$  phase decomposition. As the temperature increases from 1150 to 1300 °C, the  $\beta$  phase precipitation in the dendritic core increases and it becomes leaner and leaner in  $\beta$  stabilizing elements, thus reducing the contrast between the dendritic (bright) and inter-dendritic (dark) regions leading to the gradual decrease and disappearance of the dendritic structure. The  $\beta$  phase decomposition kinetics is similar for A2, A3, A4, A5 and A6 alloys as seen in Figs. 2, 3 and 4.

It may be observed that the  $\beta$  volume fraction in WQ is generally higher in comparison to that in the FC condition in all the alloys at all the temperatures (Table 3). The reason for the decrease in  $\beta$  volume fraction is the slow cooling in case of FC that allows sufficient time for decomposition of the  $\beta$  phase to occur, leading to a decreased  $\beta$  phase fraction in FC condition. The alloys A1 and A3 show a maximum  $\beta$  phase content of more than 12% after heat treating at 1300 °C for 4 h followed by WQ. The alloy A6 shows a highest  $\beta$  phase content of higher than 12% after heat treatment at 1200 °C for 4 h followed by FC. The higher  $\beta$  stabilization due to higher Nb and Mo in case of A6 probably helps in retaining the  $\beta$  phase even after slow cooling.

## Morphology of Phases

### B2/ $\beta$ Phase

In the alloys studied, the  $\beta$  phase appears in bright contrast at various locations such as dendritic regions, lamellar boundaries, equiaxed boundaries, within the grain and inter-phase boundaries. Different morphologies such as fine, coarse, equiaxed, irregular and lamellar structure can be observed. In the present study, dendritic  $\beta$  phase was observed upto 1300 °C in both the WQ and FC conditions for all the alloys A1, A2, A3, A4, A5 and A6 (Figs. 1, 2, 3, and 4). It clearly points to the fact that the temperature of 1300 °C is not sufficient to dissolve  $\beta$  phase completely in the solid state. At higher temperatures (1350 and 1400 °C), the morphology of  $\beta$  changes from elongated to equiaxed/blocky at the grain/colony boundaries (Figs. 1 and 3). It was also clearly observed that, as the amount of  $\beta$  stabilizing elements increased, elongated  $\beta$  was observed along and within the lamellae (Figs. 1, 2, 3, and 4).

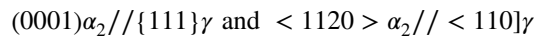
### $\alpha/\alpha_2$ Phase

The  $\alpha/\alpha_2$  phase appears in gray contrast in the BSE SEM micrographs. It forms as fine, coarse, equiaxed, lamellar, near lamellar and duplex structures. In the present alloy system, lamellar  $\alpha_2$  was observed up to 1350 °C in WQ and at all temperatures in FC condition, respectively (Figs. 1, 2, 3, and 4).

### $\gamma$ Phase

The  $\gamma$  phase is seen in dark contrast in the BSE SEM micrographs due to Al enrichment. Various morphologies such as fine, coarse, equiaxed, lamellar, near lamellar and duplex structure can be observed. Generally, it forms at inter-dendritic regions due to high amount of relatively low melting element such as aluminum, and solidifies last.

During solidification, it followed the Blackburn [9, 16] orientation relationship with  $\alpha$  phase.



From Figs. 1, 2, 3, and 4, three types of  $\gamma$  phase were observed: (a) the formation of lamellar  $\gamma$  phase from the  $\alpha$  phase as per the solid state reaction  $\alpha \rightarrow \alpha + \gamma \rightarrow \alpha_2 + \gamma$  [9]. Thus, the  $\gamma$  phase forms as alternate laths along with the  $\alpha$  phase. Generally the width of the  $\gamma$  lamellae is more than that of the  $\alpha_2$  phase, which may be due to faster growth rate of former than that of the later, (b) the other type of  $\gamma$  observed is the equiaxed  $\gamma$  phase, which results from the solid state reaction  $\beta \rightarrow \beta + \gamma$  [9]. The kinetics of  $\gamma$  phase formation from  $\beta$  is a slow, and therefore it grows in all directions and forms globular structure and (c) the  $\gamma$  phase was also seen adjoining the  $\beta$  phase (Fig. 1 a inset) which may be due to the  $\alpha + \beta \rightarrow \gamma$  solid state transformation reaction [9].

## Hardness at Various Temperatures

Hardness for all the alloys at various temperatures, i.e., at 1400, 1250, and 1150 °C in WQ and FC conditions were measured and given in Table 6 and Fig. 10. It is clearly observed that the hardness of all the alloys is high at 1400 °C followed by 1150 °C and low at 1250 °C in WQ condition, whereas no such trend is found in FC condition. Alloy A4 exhibited the highest hardness of 407 VHN at 1400 °C in WQ and alloy A6 exhibited a hardness of 329 VHN at 1150 °C in FC condition.

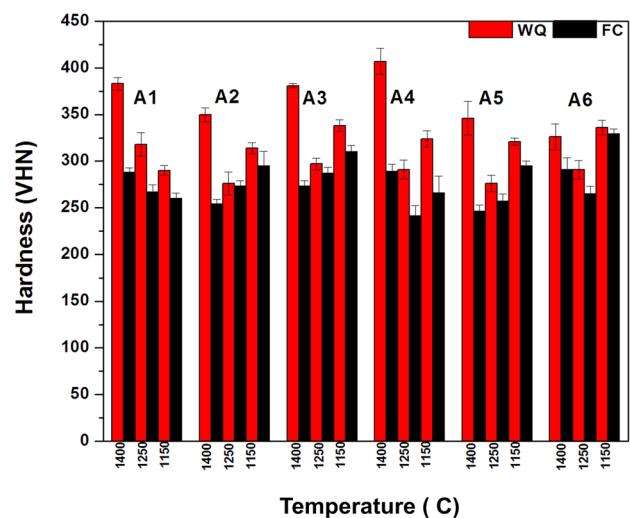


Fig. 10 Hardness values of all the alloys at various temperatures and cooling rates

The hardness of each individual phase was measured using microhardness in various conditions. The hardness of B2 phase was found to be highest at 715 VHN, whereas  $\gamma$  phase exhibited the least hardness of 378 VHN. The hardness of lamellar  $\alpha_2$  and equiaxed  $\alpha$  phases were 549 and 511 VHN, respectively. Hence, the high hardness in WQ condition (higher B2 phase fraction) in comparison to FC (Table 6 and Fig. 10) is not surprising, as it has been reported that B2 has higher hardness than that of the  $\alpha_2$  and  $\gamma$  phases [17, 18].

The hardness depends on the variation in microstructural constituents and their features such as grain size, phase fraction and morphology. It has been reported that,  $\alpha/\alpha_2$  phase has relatively higher strength than the  $\gamma$  phase [19]. Hence, the presence of higher  $\alpha/\alpha_2$  phase fraction or thicker  $\alpha/\alpha_2$  lamellae, results in higher hardness values [20]. The present alloys show  $\beta$  phase at 1400 and 1250 °C, and  $\beta/B2$  at 1150 °C temperatures (Table 5). Hence, when compared with 1250 °C, alloys at 1150 °C exhibited higher hardness in WQ condition as  $\beta/B2$  phase has higher hardness. At 1400 °C, as all the alloys lie in the two phase  $\alpha + \beta$  region (Table 6) with small amounts of  $\gamma$  phase, higher  $\alpha$  fraction may be the reason for higher hardness in all the alloys (Fig. 10). Similar trend was not observed in FC condition even with similar phase fraction when compared to WQ, which might be due to the differences in chemical constituents within B2,  $\alpha_2$  and  $\gamma$  phases and their morphologies.

## Conclusions

The phase transformation behavior of six  $\gamma$  Ti–46.5Al– $x$ Nb– $y$ Cr– $z$ Mo–0.3B alloys, where  $x=3.5, 5; y, z=0, 1, 2$  and  $x+y=2$  have been investigated as a function of temperature and two extreme cooling rates and the following conclusions can be drawn from the study:

- The micro-segregation (dendritic structure) present in as-cast condition is retained in the present  $\gamma$ -TiAl alloys after heat treatment up to a maximum temperature of 1300 °C.
- The alloy system investigated thus lies in a two phase  $\alpha + \beta$  field from about 1430 °C down to about 1288–1272 °C. A three phase region below the two phase field exists, with the eutectoid temperature lying in the range of 1155–1076 °C.
- The eutectoid transformation temperature ( $T_{eu}$ ) decreases with increase in Mo content.
- Nb addition does not appear to have a significant effect on transformation temperatures, although the eutectoid temperature appears to have decreased slightly in higher Nb containing alloys.
- The volume fraction of  $\beta/B2$  phase in water quenched condition is generally higher than in furnace cooled con-

dition for all the alloys, as in later condition sufficient time is allowed for its decomposition and it reaches its equilibrium content.

- The alloy A1 (3.5Nb–2Cr) and A3 (3.5Cr–2Mo) show the highest  $\beta/B2$  phase content at 1300 °C in water quenched condition, whereas alloy A6 (5Nb–2Mo) shows the highest  $\beta$  phase content at 1200 °C in furnace cooled condition.
- The hardness of B2 phase is the highest, followed by lamellar  $\alpha_2$ ,  $\alpha/\alpha_2$  and  $\gamma$  phases. The hardness of alloys in water quenched condition is higher when compared to that of furnace cooled samples at all the heat treatment temperatures.

**Acknowledgements** The authors are thankful to DRDO for funding this research work and to Director DMRL for granting permission to publish these results. The authors gratefully acknowledge the support from NIT Warangal.

## References

1. H.F. Chladil, H. Clemens, H. Leitner, A. Bartels, R. Gerling, F.P. Schimansky, S. Kremmer, Phase transformations in high niobium and carbon containing  $\gamma$ -TiAl based alloys. *Intermetallics* **14**, 1194–1198 (2006)
2. I. Gil, M.A. Munoz-Morris, D.G. Morris, The effect of heat treatments on the microstructural stability of the intermetallic Ti–46.5Al–2 W–0.5Si. *Intermetallics* **9**, 373–385 (2001)
3. A. Denquin, S. Naka, Phase transformation mechanisms involved in two-phase TiAl-based alloys-I. Lamellar structure formation. *Acta Mater.* **44**, 343–352 (1996)
4. S. Mayer, C. Sailer, H. Nakashima, T. Schmoelzer, T. Lippmann, P. Staron, K.D. Liss, H. Clemens, M. Takeyama, Phase equilibria and phase transformations in molybdenum-containing TiAl alloys. *Mater. Res. Soc. Symp. Proc.* **1295**, 113–118 (2011)
5. Y.W. Kim, Gamma titanium aluminides: their status and future. *JOM* **47**, 39–42 (1995)
6. S.C. Huang, in: *Structural Intermetallics*, ed by R. Darolia, J. Lewandowski, C.T. Liu, P. Martin, D. Miracle (TMS, Warrendale, 1993), p. 299
7. Y.W. Kim, Ordered intermetallic alloys, part III: gamma titanium aluminides. *JOM* **46**, 30–39 (1994)
8. U. Prasad, Q. Xu, M.C. Chaturvedi, Effect of cooling rate and manganese concentration on phase transformation in Ti-45 at.% Al based alloys. *Mater. Sci. Eng., A* **329**, 906–913 (2009)
9. N.S. Neelam, S. Banumathy, G.V.S. Nageswara Rao, A. Bhattacharjee, A.K. Singh, Solidification behavior of  $\gamma$ -aluminide Ti–46.5Al– $x$ Nb– $y$ Cr– $z$ Mo–0.3B alloys. *Vacuum* **163**, 352–359 (2019)
10. G.F. Vander Voort, Grain size measurement, in *Practical Applications of Quantitative Metallography*, ed. by J.L. McCall, J.H. Steele Jr. (American Society for Testing and Materials, Philadelphia, 1984), pp. 85–131
11. A.K. Singh, D. Banerjee, Transformations in  $\alpha_2 + \gamma$  titanium aluminide alloys containing molybdenum: Part II. Heat treatment. *Metall. Mater. Trans. A* **28A**, 1745–1753 (1997)
12. E. Schwaighofer, H. Clemens, S. Mayer, J. Lindemann, J. Klose, W. Smarsly, V. Güther, Microstructural design and mechanical

- properties of a cast and heat treated intermetallic multi-phase  $\gamma$ -TiAl based alloy. *Intermetallics* **44**, 128–140 (2014)
13. N.A. Belov, M.E. Samoshina, Influence of the thermal treatment temperature on the microstructure and phase composition of casts of  $\beta$  solidifying TNM alloy based on the Ti–Al–Nb–Mo system. *Russ. J. Non Ferrous Met.* **55**, 37–45 (2014)
  14. A.V. Kuznetsov, V.S. Sokolovskii, G.A. Salishchev, N.A. Belov, N.A. Nochovnaya, Thermodynamic modelling and experimental study of phase transformation in alloys based on  $\gamma$ -TiAl. *Met. Sci. Heat Treat.* **58**, 14–23 (2016)
  15. A. Chlupová, M. Heczko, K. Obrtlík, J. Polák, P. Roupcová, P. Beran, T. Kruml, Mechanical properties of high niobium TiAl alloys doped with Mo and C. *Mater. Des.* **99**, 284–292 (2016)
  16. F. Appel, J.D.H. Paul, M. Oehring, *Gamma Titanium Aluminide Alloys* (Wiley, Weinheim, 2011)
  17. C. Leyens, M. Peters, *Titanium and Titanium Alloys* (Wiley, Weinheim, 2003)
  18. S. Banumathy, R.K. Mandal, A.K. Singh, Hot rolling of binary Ti–Nb alloys Part II: mechanical properties anisotropy. *Int. J. Mat. Res* **102**, 208–217 (2011)
  19. F. Kong, Y. Chen, F. Yang, Effect of heat treatment on microstructures and tensile properties of as-forged Ti–45Al–5Nb–0.3Y alloy. *Intermetallics* **19**, 212–216 (2011)
  20. S.L. Semiatin, V. Seetharaman, V.K. Jain, Microstructure during conventional and isothermal hot forging of a near gamma titanium aluminide. *Metall. Mater. Trans. A* **25**, 2753–2768 (1994)

**Publisher's Note** Springer Nature remains neutral with regard to jurisdictional claims in published maps and institutional affiliations.